

Refined Analysis of an L-Shaped Cap Beam Based on the Spatial Finite Element Method

Yan Dang

Tongji Architectural Design (Group) Co., Ltd., Shanghai 200092, China.
Correspondence: 935799346@qq.com

Abstract: The focus of this study is the transition pier of the main approach bridge in a newly constructed project in Chengdu. It begins by introducing the configuration strategy for the prestressed tendon layout. A comparative analysis of sectional stresses is then conducted under prestress loading conditions and at the completed bridge stage, using both spatial frame models and spatial solid models. Special emphasis is placed on investigating the torsional shear stress induced by structural and loading asymmetry in the L-shaped cap beam. The results show that the spatial frame models could meet practical engineering requirements. These findings provide valuable references for the design analysis of similar engineering projects.

Keywords: L-shaped cap beam; spatial finite element; refined analysis; torsional shear stress; prestress

1 Introduction

At transition piers of main—approach bridges, significant elevation differences between the main span and approach girders often make height coordination through superstructure adjustments alone impractical. As a result, L-shaped cap beams (high–low cap beams) are frequently used to accommodate vertical discrepancies. However, the inherent asymmetry of L-shaped cross-sections creates substantial eccentricity between the centroid and shear center. When combined with unequal loading from the main and approach spans, this asymmetry results in non-uniform stress distribution across the section, significant torsional shear stresses, and pronounced three-dimensional force flow patterns [1,2]. Current research methodologies [3–5] primarily employ spatial solid finite element models for analysis. Despite providing detailed stress contours, these models face significant limitations, including high computational costs—in terms of both resources and time—and difficulties in directly correlating stress results with code verification parameters. In this study, an optimized spatial frame model with enhanced modeling efficiency is proposed. Comparative analysis with spatial solid models demonstrates that the proposed methodology achieves sufficient accuracy to meet practical engineering requirements.

2 Structural Overview

2.1 Engineering Characteristics

The main bridge is a single-pylon cable-stayed structure with a spatial cable plane and a main span of 238 m. It features an integral steel box girder cross-section, with a girder height of 3.7 m at the road centerline and a total bridge width of 64 m. The approach bridge consists of 30 m prestressed concrete (PC) small box girders with a girder height of 1.7 m. Except for the steel box girder of the main bridge, all other structures are designed with separated decks.

The transition pier cap beam (as shown in Figure 2) has a single-span length of 30.75 m. The top surface of the cap beam features a 2% unidirectional slope on the approach bridge side and a flat surface on the main bridge side. The overhang lengths are 6.75 m on the outer side and 9.4 m on the inner side. The cap beam adopts

Citation: Dang, Y. Refined Analysis of an L-Shaped Cap Beam Based on the Spatial Finite Element Method. *Prestress Technology* 2025, 2, 43–53.
<https://doi.org/10.59238/j.pt.2025.02.004>

Received: 21/05/2025

Accepted: 17/06/2025

Published: 30/06/2025

Publisher's Note: Prestress technology stays neutral with regard to jurisdictional claims in published maps and institutional affiliations.



Copyright: © 2025 by the authors. Submitted for possible open access publication under the terms and conditions of the Creative Commons Attribution (CC BY) license (<https://creativecommons.org/licenses/by/4.0/>).

an L-shaped stepped section (high–low cap beams, as illustrated in Figure 3). On the main bridge side, the beam has a height of 1.7 m and a width of 1.93 m. On the approach bridge side, the beam height varies from 2.285 to 2.695 m, with a width of 1.57 m. The pier itself is an irregular-shaped structure with a height of 23.5 m.

Material Specifications: C50 concrete is used for the cap beam, C40 concrete for the pier, and C35 concrete for the pile cap.

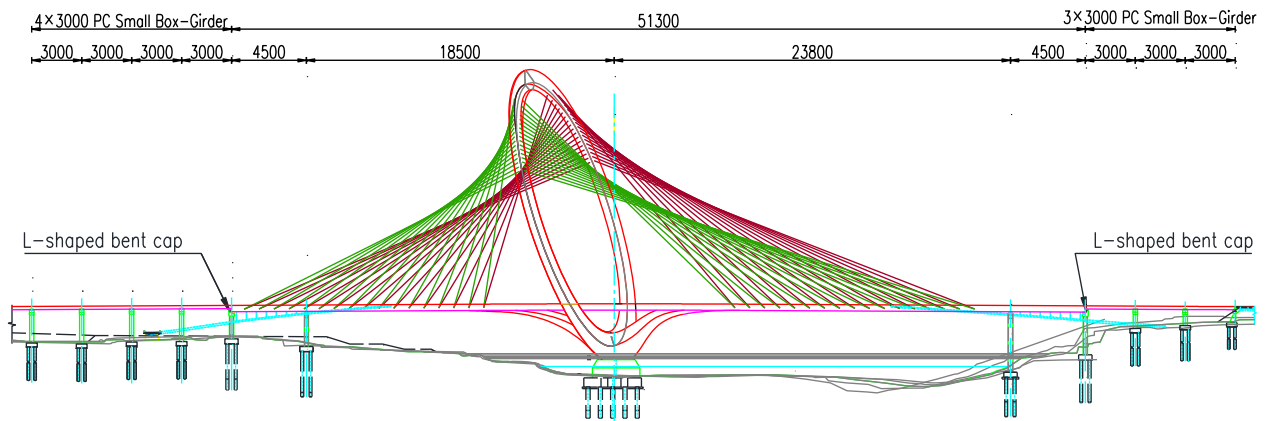


Figure 1 Overall layout of the bridge (unit: cm)

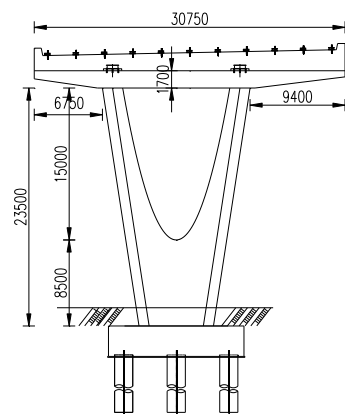


Figure 2 Elevation of cap beam (unit: mm)

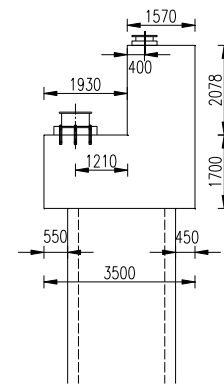


Figure 3 Cross-section of cap beam (unit: mm)

2.2 Load Application Conditions

2.2.1 Dead Loads

- (1) The self-weight of the cap beam, pier, and pile cap is included.
- (2) For the approach bridge, Phase I dead loads include the weights of the prefabricated and cast-in-situ small box girders. Phase II dead loads account for the weights of the pavement, railings, and median strips, which are considered to act on the transverse positions of the bridge deck.
- (3) Dead loads for Phases I and II of the main bridge are applied as calculated support reactions from the superstructure analysis.
- (4) The abutment blocks on the approach bridge side are modeled as nodal loads directly applied to both ends of the high side (small box girder side) of the L-shaped cap beam. The self-weight and Phase II dead loads of the approach bridge are applied through bearing nodes on the high side of the L-shaped cap beam, while the self-weight and Phase II dead loads of the main bridge are applied through bearing nodes on the low side (steel girder side) of the cap beam.

2.2.2 Temperature Loads

- (1) According to Clause 4.3.12 of the “General Specifications for Design of Highway Bridges and Culverts” (JTG D60—2015) [6], both the overall temperature rise and drop are specified as 20 °C.

- (2) Gradient temperature rise/drop in the main bridge structure and cable temperature differentials are included in the superstructure reaction calculations, with uniform temperature variation in the cap beam–pier integral system considered simultaneously.

2.2.3 Live Loads

- (1) Approach bridge vehicle live loads are determined in accordance with Clause 4.3.1 of the “General Specifications for Design of Highway Bridges and Culverts” (JTG D60–2015), with maximum single-lane longitudinal reactions identified using longitudinal influence lines.
- (2) For the approach bridge, reaction forces at beam ends under a crowd uniform live load are calculated in accordance with Clause 10.0.5 of the “Code for Design of the Municipal Bridge” (CJJ 11–2011), with the load applied through transverse movement.
- (3) Main bridge live loads are extracted as the maximum support reactions from the longitudinal analytical model and are applied inversely as static loads at the main bridge bearing positions.

2.2.4 Special Considerations

The most critical support reactions under live loads, pedestrian loads, uniform temperature variation, gradient temperature effects, cable temperature differentials, and wind loads on the main bridge are calculated through superstructure analysis and applied in reverse as static loads at the cap beam bearing nodes. Since the transverse bearing adjacent to the road centerline on the main girder is a fixed bearing, lateral reactions generated at this bearing under all load combinations are explicitly included in the load application.

3 Prestressing Steel Tendon Design

3.1 Tendon Arrangement Concept

3.1.1 Initial Concept

A symmetrical transverse tendon arrangement was initially proposed at the centroid of the overall cap beam section, near the upper edge of the low-side girder (as shown in Figure 4). Although this configuration generates only vertical bending moments under prestressing loads, it results in insufficient compressive stress at the upper edge of the high side of the L-shaped cap beam due to its distance from the tendons. Conversely, excessive compressive stress develops at the upper edge of the low side of the cap beam.

3.1.2 Revised Concept I

In this approach (Figure 5), the tendons on the high side of the L-shaped cap beam are vertically shifted upward. Although this mitigates the compressive stress deficiency at the upper edge of the high side, it introduces critical issues:

- (1) Excessive tensile stresses develop at the bottom of the overall cap beam.
- (2) A significant stress differential emerges between the bottoms of the high and low sides of the L-shaped cap beam.
- (3) Additional horizontal bending moments arise under prestressing loads, leading to potential cracking at the bottom and lateral surfaces of the high side of the L-shaped cap beam [7].

3.1.3 Revised Concept II

Based on the mechanical characteristics of the transition pier cap beam in this project:

- (1) The bearings on the main bridge side are located near the pier column. Under the reaction force from the main bridge side, the V-shaped pier induces significant tensile stress in the lower region of the cap beam.
- (2) The upper edge at midspan on the high side of the L-shaped cap beam consistently remains in tension.

- (3) The above analysis further informs the improvement strategy:
- (4) Cap beam midspan: Arrange prestressing tendons in the lower section of the cap beam and the upper section of the high side of the L-shaped cap beam. This ensures that compressive stress develops across the entire cap beam cross-section.
- (5) Cap beam ends: Since the bottom region of the cap beam ends consistently experiences compressive stress, placing tendons in the lower section would further increase compressive stress at this location. Therefore, during anchoring of the upper tendons in the high side of the L-shaped cap beam, anchorages should be positioned in the upper-middle portion of the cross-section.

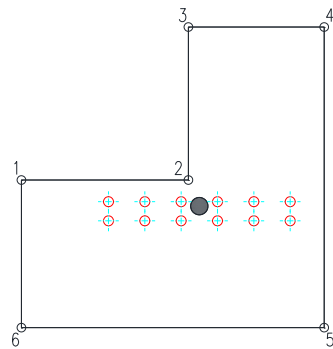


Figure 4 Initial concept: tendon layout

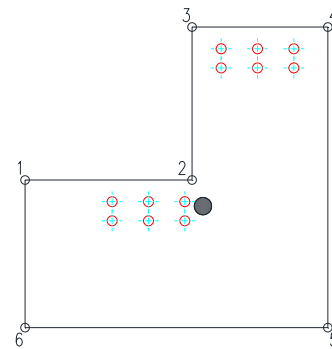


Figure 5 Revised concept I: tendon layout

3.2 Final Tendon Configuration

Through iterative analysis, the final tendon layout (Figure 6) employs 21 – $\varnothing^s 15.2$ low-relaxation prestressing strands (i.e., 21 prestressing tendons with a diameter of 15.2 mm)

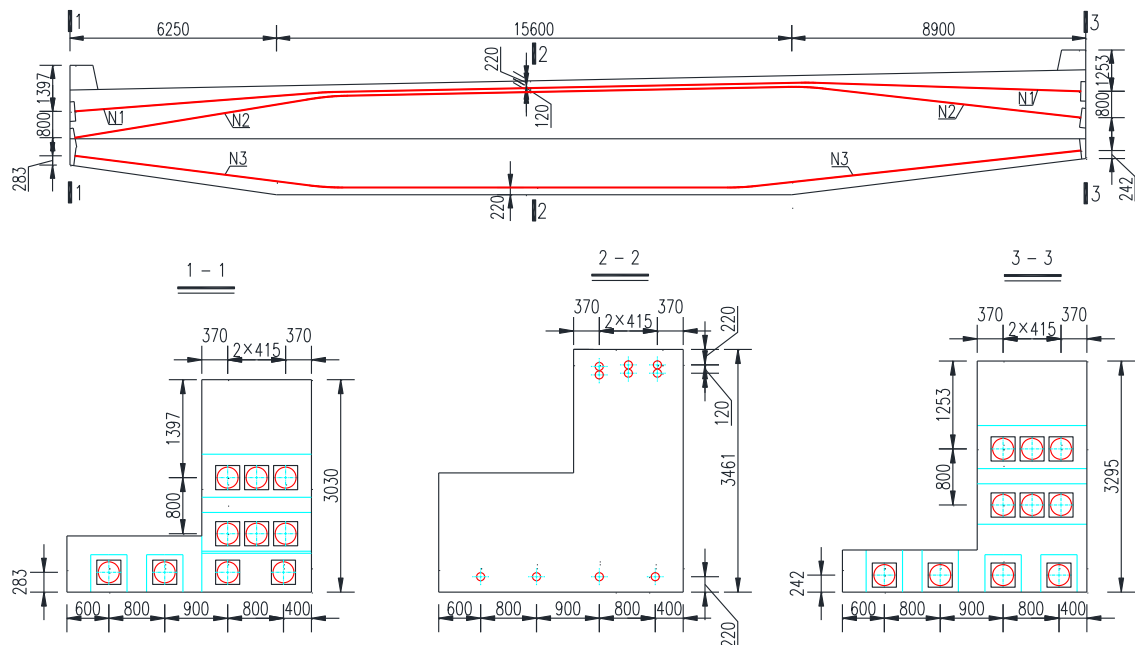


Figure 6 Revised concept II: final tendon layout (unit: mm)

The cap beam cross-section is reinforced with one layer of HRB400 main reinforcement bars (32 mm diameter @100 mm spacing) at both the top and bottom. Stirrups consist of 16mm HRB400 steel arranged in a 10-legged configuration at 100mm spacing. Given the severe structural and loading asymmetry between the main bridge and approach bridge sides, the combined torsional resistance of the stirrups and main reinforcement has been verified.

3.3 Mid-Span Stress Comparison

Using the final tendon configuration as a benchmark, three tendon arrangements were analyzed using spatial frame models, each with an equal total number of tendons. The corner stresses at the mid-span section under prestressing loads are compared in Table 1.

Table 1 Corner stresses at the mid-span section under prestressing loads for three schemes

Tendon Arrangement	Corner 1 Stress (MPa)	Corner 4 Stress (MPa)	Corner 5 Stress (MPa)
Initial	-8.2	-1.9	-1.4
Revised I	-2.3	-3.5	-0.4
Revised II	-1.8	-5.2	-3.7

Note: Negative values indicate compressive stress.

The comparative analysis demonstrates that Revised Concept II provides a superior compressive stress distribution across all mid-span corners, with adequate stress reserves at critical locations.

4 FEM Model

4.1 Research Method

This study establishes spatial frame models and solid models. The research method is as follows:

- (1) Comparative stress analysis at cap beam corner nodes under two conditions—prestressing loads only vs. completed bridge state—to validate the reliability of the spatial frame models;
- (2) Analysis of stress distribution variations across different cross-sectional locations in the completed bridge state;
- (3) Evaluation of torsional shear stress effects on the cross-section under the completed bridge state.

4.2 Spatial Frame Model

- (1) The spatial frame model was developed using Midas Civil (a structural analysis software). Key modeling strategies include:
 - a) Bridge piers and cap beams are simulated using beam elements;
 - b) Virtual deck elements are created to simulate transverse vehicular loading on the approach bridge side;
 - c) Master–slave constraints are applied at actual bearing positions to connect the deck elements with the cap beam structural elements;
 - d) Element offsets are used to model bearing reactions on the main bridge side.
- (2) All load applications account for eccentricity to ensure alignment with actual structural behavior.
- (3) Primary load cases considered:
 - a) Prestressing Load Case: Includes only the substructure self-weight and prestressing forces.
 - b) Standard Load Combination: Includes all dead loads from the superstructure and substructure, as well as vehicle loads, pedestrian loads, temperature effects, and wind loads on the main bridge.

4.3 Spatial Solid Model

A spatial solid model of the bridge cap beam was developed using Midas FEA (a finite element analysis software) to validate selected computational results from the aforementioned spatial frame model. All load applications were applied consistently with those in the spatial frame model, including the types of loads and methods of application.

5 Computational Results Analysis

This structural analysis uniformly applied basic load combinations to verify the bearing capacity limit state of the cap beam, while employing frequent and quasi-permanent combinations to assess the serviceability limit state [6,8]. Under serviceability limit conditions, the cap beam was designed as a fully prestressed concrete member, with the following stress limits: maximum tensile stress at normal sections $\sigma_t \leq 1.85$ MPa; maximum principal tensile stress at inclined sections $\sigma_{tp} \leq 1.33$ MPa; and maximum compressive stress at normal sections $\sigma_c \leq 16.2$ MPa.

5.1 Comparison Between Spatial Frame and Solid Models

To validate the reliability of the spatial frame model, a spatial solid model was developed to simulate two critical loading phases: the prestressing load case (Construction Stage) and the completed bridge state (Operational Stage). Stress values at three key corners (4, 5, and 6) of the cap beam were compared between the two models (Figures 7 - 9).

Notably, stress concentrations near the cap beam ends caused by tendon anchorage in the solid model were excluded from the analysis by assigning a uniform stress value of zero for comparison purposes.

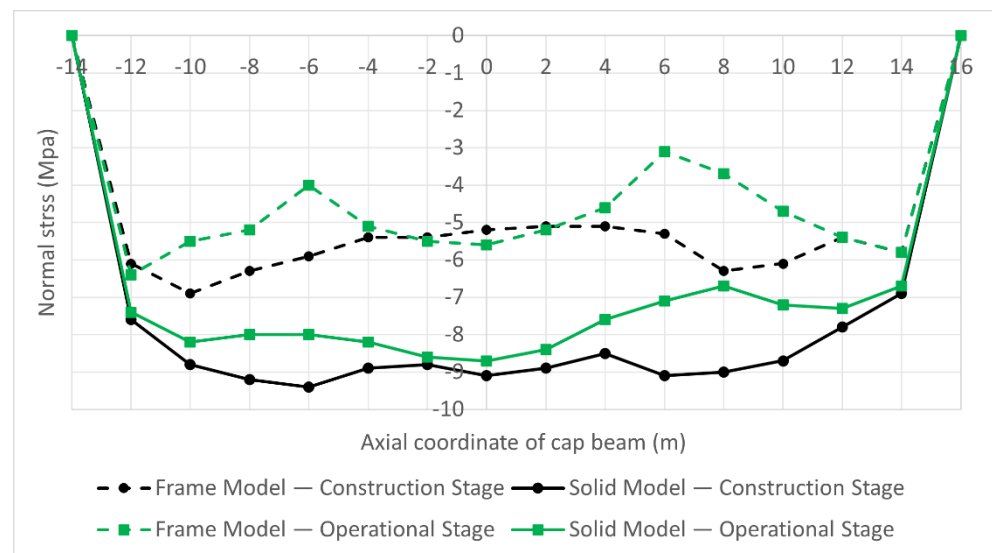


Figure 7 Difference in stress at Corner 4 of the cap beam under different models and load cases

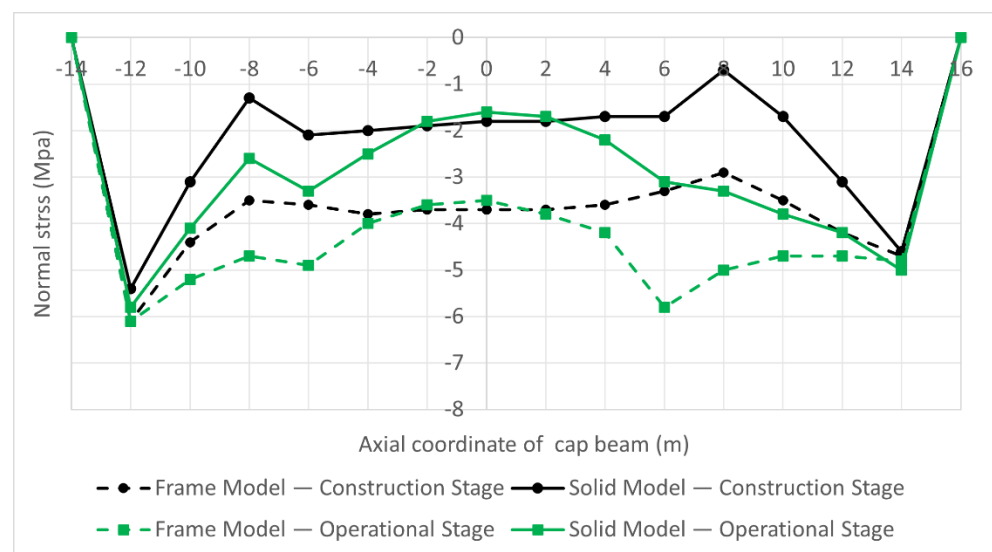


Figure 8 Difference in stress at Corner 5 of the cap beam under different models and load cases

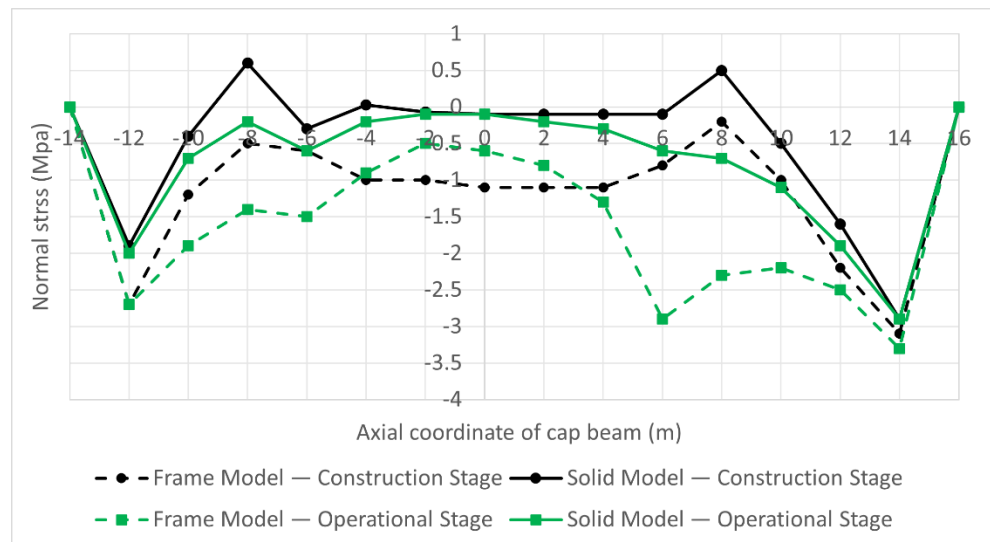


Figure 9 Difference in stress at Corner 6 of the cap beam under different models and load cases

Based on the above computational results, the following conclusions can be drawn:

- (1) The stress results from the spatial frame model differ to some extent from those of the spatial solid model. However, under identical loading conditions, the variation of normal stress along the axis of the cap beam at corresponding cross-sectional positions is consistent between the two models.
- (2) Under prestressing loads alone (Construction Stage), both models indicate that the upper edge of the cap beam is subjected to compressive stress. The spatial solid model shows higher compressive stress values, with a maximum difference of 3.9 MPa. The lower edge is also generally under compressive stress, but the spatial solid model indicates lower compressive stress values. The maximum differences are 1.0 MPa at the left-side corner (Corner 5) and 2.2 MPa at the right-side corner (Corner 6). Additionally, in the spatial solid model, tensile stress appears near the pier at the lower edge.
- (3) In the completed bridge state (Operational Stage), the compressive stress differences between the two models remain largely consistent with those observed under prestressing loads. The upper edge experiences compressive stress, with the spatial solid model indicating higher values, and a maximum stress difference of 4.0 MPa. Similarly, the lower edge is under compressive stress, but the spatial solid model shows lower compressive stress values. The maximum stress differences are 2.3 MPa at the left-side corner (Corner 5) and 2.7 MPa at the right-side corner (Corner 6).

The differences in computational results between the two models mainly arise from the fact that, although the spatial frame model accurately simulates the spatial distribution of loads, its inherent reliance on the plane section assumption—as characteristic of beam elements—leads to discrepancies from the actual stress conditions experienced by the cap beam.

Based on the above computational results, the following conclusions can be drawn:

- (1) There is a significant difference in the upper edge stress between the two models; however, in all cases, the compressive stress calculated by the spatial frame model is lower. From an engineering design perspective, relying on the spatial frame model results remains on the safe side.
- (2) For the lower edge, except within the pier width range, the overall stress differences between the two models are relatively small. This is due to the

spatial frame model’s inability to simulate the moment reduction effect at the upper edge of the cap beam [9]. In practical engineering applications, it is advisable to apply empirical adjustments to the stress results in this region.

- (3) Overall, the computational results of the spatial frame model generally meet the requirements for practical engineering calculations.

5.2 Stress Variation Across Cross-Sectional Locations

Building on the validated reliability of the spatial frame model, this section investigates the stress distribution patterns at six critical corners of the L-shaped cap beam under the completed bridge state (Operational Stage), as shown in Figure 10. The analysis focuses on normal stress distribution using the spatial frame model.

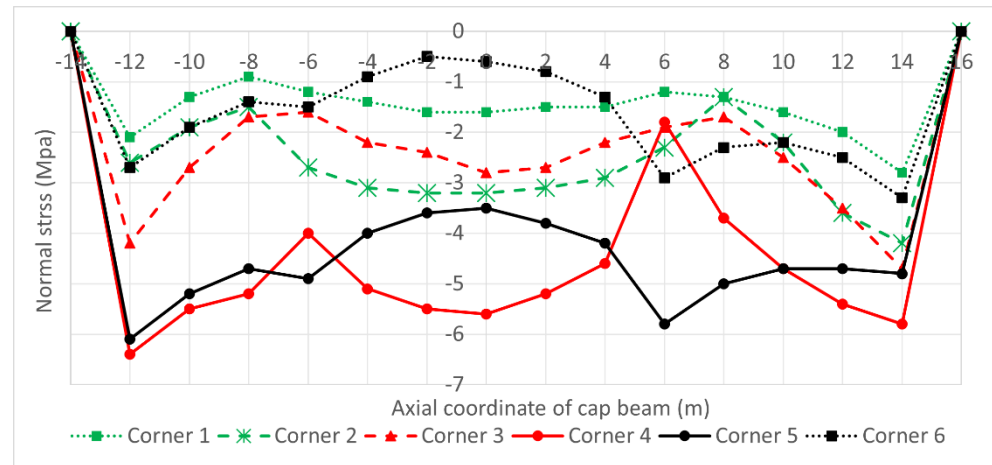


Figure 10 Stress distribution at different corners of the cap beam under the operational stage

From the above computational results, the following conclusions can be drawn:

- (1) In the completed bridge state, the stress variation along the axis on both sides of the upper edge of the lower side of the cap beam (Corner 1 and Corner 2) remains consistent. In the midspan region between the two piers, Corner 2 exhibits higher compressive stress reserves than Corner 1. This is due to the prestressing force from the tendons being applied closer to Corner 2 in the midspan area of the upper zone on the higher side of the cap beam, providing greater compressive stress reserves to Corner 2. In the cantilever sections, the stress difference between the two corner points is smaller, which is attributed to the low height of the cap beam on the lower side and the concentrated anchoring of tendons in this area, resulting in minimal stress variation.
- (2) In the completed bridge state, the stress variation along the axis on both sides of the upper edge of the higher side of the cap beam (Corner 3 and Corner 4) follows a pattern similar to that of the lower side of the cap beam. In the midspan region, the compressive stress at Corner 4 is nearly twice that at Corner 3. This is because, under the main bridge load, the reaction forces from the irregular main pier cause the lower side of cap beam to bear more tensile stress. Since this tensile stress is closer to Corner 3, it leads to greater tensile stress at Corner 3.
- (3) In the completed bridge state, the tensile stress differences on both sides of the lower edge (Corner 5 and 6) are more pronounced. Based on the stress calculation results under prestressing loads discussed earlier, the main reason lies in the arrangement of steel strands, which provides greater compressive stress reserves at Corner 5 and less at Corner 6.
- (4) Considering the stress distribution at all corner points of the cap beam, the arrangement of steel strands ensures that the higher side of the cap beam has better compressive stress reserves. Although the lower side has relatively

smaller compressive stress reserves due to its limited height, the prestress generated by the strands arranged along the lower edge is effectively transferred to the upper edge of the lower side of the cap beam, ensuring it remains under compression.

The stress distribution along both the upper and lower edges of the L-shaped cap beam is highly uneven. The spatial frame model can simulate these variations, producing results that are similar to, yet relatively conservative compared to, those of the spatial solid model. Given its faster modeling and computation efficiency, the spatial frame model is more suitable for assisting in the design of prestressed steel strands.

5.3 Torsional Shear Stress Analysis

Based on the computational results of the spatial frame model (Figure 11) under the completed bridge state, the maximum torsional shear stress in the cap beam occurs at the beam ends. The torsional shear stress at the outer beam end (the outside of the twin bridges) is 1.9 MPa, while at the inner beam end (the inside of the twin bridges), it is 0.9 MPa. Due to the inherent characteristics of the frame model, the detailed distribution of torsional shear stress across the beam end section cannot be obtained from the spatial frame model.

In the spatial solid model (Figure 12), it is clearly observed that the maximum torsional shear stress on the beam end section occurs at Corner 5, with a value of 2.0 MPa at the outer beam end and 1.8 MPa at the inner beam end.

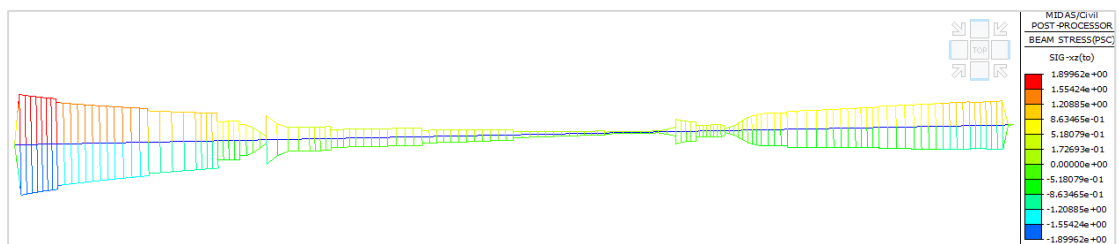


Figure 11 Torsional shear stress from the spatial frame model (unit: MPa)

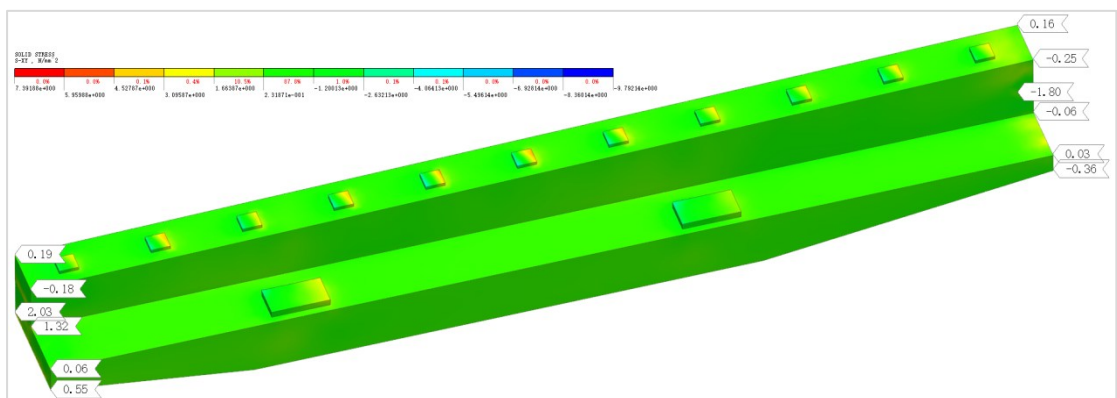


Figure 12 Torsional shear stress from the spatial solid model (unit: MPa)

It can therefore be concluded that the maximum torsional shear stress of 2.0 MPa is caused by the double asymmetry of both the structure and the loading, and that the analysis results from the spatial frame model are generally reliable.

If the traditional reinforcement arrangement for cap beams were adopted, the structure's torsional capacity would not meet code requirements. In this design, torsional capacity was the controlling factor for the entire cap beam's transverse reinforcement configuration. The stirrups were reinforced using 10-legged HRB400 steel bars with a diameter of 16 mm spaced at 100 mm. A verification calculation of

the torsional capacity, considering both stirrups and longitudinal reinforcement, was conducted, and the results indicate that the designed torsional reinforcement meets code requirements [10].

6 Conclusions

This study conducted comprehensive analyses of the transition pier cap beam of a new bridge project in Chengdu, leading to the following key conclusions:

- (1) The tendon arrangement based on Revised Concept II meets the verification requirements of the “Specifications for Design of Highway Reinforced Concrete and Prestressed Concrete Bridges and Culverts” (JTG 3362—2018) under specified load combinations and stress control criteria.
- (2) For large L-shaped cap beams, preliminary conceptual analysis of superstructure loads can guide trial tendon layouts, which are then refined through iterative modeling to achieve optimized tendon profiles.
- (3) While spatial frame models inherently assume plane sections and thus deviate slightly from the real stress states captured by solid models, these deviations remain within acceptable engineering tolerances and satisfy code requirements for strength and stress verification.
- (4) The spatial frame model, combined with refined modeling techniques, provides sufficient accuracy for practical engineering applications. For complex cases, supplementary solid modeling is recommended for further verification and optimization.
- (5) Due to structural and loading asymmetry, torsional shear stress in L-shaped cap beams cannot be neglected and must be explicitly addressed in the design.

Conflict of interest: All the authors disclosed no relevant relationships.

Data availability statement: The data that support the findings of this study are available from the corresponding author, Dang, upon reasonable request.

References

1. Wei, B. Spatial Stress Analysis of L-shaped Bent Cap for Medium and Small Span Bridges. Master, Chang'an University, 2011.
2. Wang, Z.; Gao, J.; Wei, B.; Wu, R. Defects and Maintenance Measures of L-shaped Bent Cap of Urban Bridge. *Municipal Engineering Technology* **2021**, *39*, 46-49, doi:10.19922/j.1009-7767.2021.02.046.
3. Sun, H.; Gao, M.; Li, J. The Analysis of Large Cantilever L-shaped Prestressed Concrete Bent Cap Stress. *Shandong Jiaotong Keji* **2014**, *38-39*, 42, doi:10.3969/j.issn.1673-8942.2014.01.013.
4. Chen, Z. Load Characteristics and Reinforcement Methods of Double Cantilever L-shaped Prestressed Concrete Bent Caps. *Urban Roads Bridges & Flood Control* **2021**, *55-58*, 77, doi:10.16799/j.cnki.csdqyfh.2021.03.017.
5. Wu, D.; Zhang, L. Solid Calculation and Analysis of L-shaped Reinforced Concrete Bent Cap Based on FEA NX. *Shandong Jiaotong Keji* **2023**, *73-77*, doi:10.3969/j.issn.1673-8942.2023.04.021.
6. Ministry of Transport of the People's Republic of China JTG D60—2015 General Specifications for Design of Highway Bridges and Culverts. China Communications Press: Beijing, 2015.
7. Shi, Y. Analysis on the Cause of Cracks of a Cap Beam and Study on Reinforcement Measures. Master, Wuhan University of Technology, 2019.
8. Ministry of Transport of the People's Republic of China JTG 3362—2018 Specifications for Design of Highway Reinforced Concrete and Prestressed Concrete Bridges and Culverts. China Communications Press: Beijing, 2018.
9. Hu, Z.; Zhang, S. Experiment and Analysis on Mechanical Behavior at Root of Large Cantilever PC Bent Cap. *Journal of Harbin Institute of Technology* **2025**, *57*, 55-68, doi:10.11918/202307017.
10. Cen, G. Research on the Load Analysis of Bent Caps on Transition Piers Based on Tension-Compression Rod Model. Master, Guizhou University, 2021.

AUTHOR BIOGRAPHIES



Yan Dang

M.E., Engineer. Graduated from Tongji University in 2017.

Working at Tongji Architectural Design (Group) Co., Ltd.

Research Direction: Bridge Structure Design, Engineering Investigation.

Email: 935799346@qq.com